Journal of Pharmaceutical Sciences 106 (2017) 1905-1916

Contents lists available at ScienceDirect

Journal of Pharmaceutical Sciences

journal homepage: www.jpharmsci.org

Pharmacokinetics, Pharmacodynamics and Drug Transport and Metabolism

Application of an NLME–Stochastic Deconvolution Approach to Level A IVIVC Modeling

Maziar Kakhi [1,*], Sandra Suarez-Sharp [1], Terry Shepard [2], Jason Chittenden [3]

[1] Food and Drug Administration, 10903 New Hampshire Avenue, Silver Spring, Maryland 20993
[2] Medicines and Healthcare Products Regulatory Agency, 151 Buckingham Palace Road, London SW1W 9SZ, UK
[3] qPharmetra LLC, Andover, Massachussetts 01810

ARTICLE INFO

Article history:
Received 6 February 2017
Revised 28 February 2017
Accepted 14 March 2017
Available online 22 March 2017

Keywords:
2-stage
level A *in vitro/in vivo* correlation (IVIVC)
numerical/stochastic deconvolution
population pharmacokinetics
nonlinear mixed-effects (NLME) modeling

ABSTRACT

Stochastic deconvolution is a parameter estimation method that calculates drug absorption using a nonlinear mixed-effects model in which the random effects associated with absorption represent a Wiener process. The present work compares (1) stochastic deconvolution and (2) numerical deconvolution, using clinical pharmacokinetic (PK) data generated for an *in vitro–in vivo* correlation (IVIVC) study of extended release (ER) formulations of a Biopharmaceutics Classification System class III drug substance. The preliminary analysis found that numerical and stochastic deconvolution yielded superimposable fraction absorbed (F_{abs}) versus time profiles when supplied with exactly the same externally determined unit impulse response parameters. In a separate analysis, a full population-PK/stochastic deconvolution was applied to the clinical PK data. Scenarios were considered in which immediate release (IR) data were either retained or excluded to inform parameter estimation. The resulting F_{abs} profiles were then used to model level A IVIVCs. All the considered stochastic deconvolution scenarios, and numerical deconvolution, yielded on average similar results with respect to the IVIVC validation. These results could be achieved with stochastic deconvolution without recourse to IR data. Unlike numerical deconvolution, this also implies that in crossover studies where certain individuals do not receive an IR treatment, their ER data alone can still be included as part of the IVIVC analysis.

Published by Elsevier Inc. on behalf of the American Pharmacists Association.

Abbreviations used: BA, bioavailability; DTC, deconvolution through convolution; ER, extended release; FID, formulation identifier (1 = fast, 2 = medium, 3 = slow, 4 = IR); FOCE-LB, first-order conditional estimation–Lindstrom/Bates method; FOCE-ELS, first-order conditional estimation—extended least-squares method; GI, gastrointestinal; IR, immediate release; IVIVC, *in vitro–in vivo* correlation; NLME, nonlinear mixed effects; ODE, ordinary differential equation; %PE, percentage prediction error; PK, pharmacokinetic(s); UIR, unit impulse response; A_a (mg), amount of drug in absorption compartment; $\overline{A}_a$(mg), IVIVC-predicted averaged amount of drug in absorption compartment; A_1 (mg), amount of drug in central compartment; $\overline{A}_1$ (mg), IVIVC-predicted averaged amount of drug in central compartment; A_2 (mg), amount of drug in peripheral compartment; $\overline{A}_2$ (mg), IVIVC-predicted averaged amount of drug in peripheral compartment; A_s (−), absorption scale factor in IVIVC model specification; AUC_{last} (ng h/mL), area under the concentration-time curve up to the last observation; b (−), shape parameter (Weibull distribution); B_i (ng/mL), pre-exponential coefficient in polyexponential model for extra-vascular PK data fit resulting from IR dosage form; C_1 (ng/mL), concentration of drug in central compartment; $\overline{C}_1$ (ng/mL), IVIVC-predicted averaged plasma concentration of drug in central compartment; C_p (ng/mL), concentration of drug in blood plasma (same as C_1); C_{max} (ng/mL), maximum concentration from blood plasma data; D (mg), dose of administered drug (100 mg for all formulations); F_{abs} (−), fraction of drug appearing in systemic circulation; F_{diss} (−), fraction of drug dissolved in the designated *in vitro* system; $F_{diss,\infty}$ (−), fraction of drug dissolved at $t_{vitro} \to \infty$ (Weibull distribution); F_{rel} (−), fraction of drug released from the formulation in the GI fluids; k_{01} (h^{-1}), first-order absorption coefficient associated with fit of IR data; k_{12} (h^{-1}), rate constant for mass transfer from central to peripheral compartments; k_{21} (h^{-1}), rate constant for mass transfer from peripheral to central compartments; k_a (h^{-1}), first-order absorption coefficient; k_e (h^{-1}), first-order elimination rate coefficient; $\overline{k}_e$ (h^{-1}), log-mean of the post hoc estimates of subject elimination rate coefficients; N (−), number of subjects; $\overline{T}_{diss}$ (h), scale parameter/mean dissolution time (Weibull distribution); t (h), time after dose; t_{vitro} (h), time elapsed in *in vitro* dissolution study; t_{RAT} (h), relative actual time; T_s (−), time scaling factor in model IVIVC; V_1 (L), volume of distribution of central compartment scaled by absolute BA; $\overline{V}_1$ (L), log-mean of the post hoc estimates of subject volume of distribution of central compartment; V_{ss} (L), volume of distribution at steady state; w ($h^{-1/2}$), normally distributed random variable associated with Wiener increment; β_i (h^{-1}), exponents in polyexponential UIR approximation fitted directly to IR data; η_{k_a} (−), random effect for absorption rate coefficient; η_{k_e} (−), random effect for elimination rate coefficient; η_{V_1} (−), random effect for volume of distribution; $\theta_{k_{12}}$ (h^{-1}), fixed effect for rate constant of mass transfer from central to peripheral compartments; $\theta_{k_{21}}$ (h^{-1}), fixed effect for rate constant of mass transfer from peripheral to central compartments; θ_{k_a} (h^{-1}), fixed effect for absorption rate coefficient; θ_{k_e} (h^{-1}), fixed effect for elimination rate coefficient; θ_{V_1} (L), fixed effect for volume of distribution; σ_w ($h^{-1/2}$), standard deviation of random walk.

Disclaimer: The views expressed in this article are those of the authors and do not reflect the opinion nor the policy of the FDA or Medicines and Healthcare Products Regulatory Agency.

Conflicts of interest: The authors have declared that there is no conflict of interest.

* *Correspondence to:* Maziar Kakhi (Telephone: +1-301-796-0082).
E-mail address: maziar.kakhi@fda.hhs.gov (M. Kakhi).

http://dx.doi.org/10.1016/j.xphs.2017.03.015
0022-3549/Published by Elsevier Inc. on behalf of the American Pharmacists Association.

Introduction

A "level A" *in vitro–in vivo* correlation (IVIVC) provides a quantitative mapping between the entire *in vitro* release time course and the entire *in vivo* response time course.[1] In more practical terms, the designated *in vitro* method can serve as a surrogate for *in vivo* clinical trials (i.e., bioequivalence studies) under certain circumstances. The utility of an IVIVC relies, in part, on its ability to guide drug product development so as to reduce redundant formulation prototyping and clinical testing.[2] An approved IVIVC may be invoked as part of a biowaiver request for certain types of post-approval manufacturing changes.[3] From a regulatory perspective, a validated level A IVIVC is expected to meet a set of criteria[4] and an important aspect of the regulatory review process is to assess an IVIVC's scientific soundness, predictive robustness, and accuracy.

For solid oral dosage forms, which are the focus of the present study, the aforementioned *in vivo* response in 2-stage (deconvolution based) IVIVC approaches is either the fraction of drug released from the formulation in the gastrointestinal (GI) fluids (referred to as "*in vivo* dissolution"—F_{rel}), or the fraction of drug appearing in systemic circulation (referred to as "fraction absorbed"—F_{abs}). Neither F_{rel} nor F_{abs} are typically reported as experimentally measured data. Indeed, they have to be calculated based on some absorption modeling approach.

The *in vitro* aspect of IVIVC modeling requires particular attention. The predictive value of the quantitative linkage defining an IVIVC is in part underpinned by the bio-predictive power of the *in vitro* dissolution method. If the dissolution method inadequately mimics the time course of the *in vivo* property of interest (e.g., cumulative amount absorbed), even the most well-characterized absorption model may prove inadequate to support a predictively accurate IVIVC.

In the present work, an approach to IVIVC development is presented based on a method referred to as "stochastic deconvolution." A more detailed introduction to stochastic deconvolution, as used here, is described in Kakhi and Chittenden.[5] In summary, stochastic deconvolution involves a system of ordinary differential equations (ODEs) representative of a mass balance in traditional compartmental pharmacokinetics (PK) coupled to a Wiener process for tracking a time-dependent absorption rate coefficient. The entire mathematical framework is embedded in a nonlinear mixed-effects (NLME) population PK formalism.

With stochastic deconvolution, it was previously demonstrated[5] that using simulated plasma concentration–time data (generated using an *a priori* known absorption profile), it was possible to recover the very same absorption profile for 3 types of PK systems, namely (1) a linear, time-invariant system, (2) a nonlinear system based on Michaelis–Menten kinetics, and (3) a linear, time-variant system representative of enterohepatic circulation. Cases (2) and (3) are particularly notable because classical numerical deconvolution would have been inapplicable under those circumstances.

In the study presented here, stochastic deconvolution has been applied to experimental (as opposed to simulated) clinical PK data stemming from a regulatory submission. This same data set has been described and analyzed using 2-stage numerical deconvolution, and these results have been reported elsewhere.[6] Consequently, the present work builds on earlier efforts with the overall goal of systematically evaluating the applicability, accuracy, and utility of stochastic deconvolution in the context of IVIVC development.

Materials and Methods

Introduction

The drug product being evaluated in this study is an extended release (ER) tablet formulation approved by the Food and Drug Administration (FDA). The drug substance is understood to exhibit linear PK over a dose range of 100-400 mg and is considered highly water soluble. Immediate release (IR) formulations of this drug substance are reported to have an absolute bioavailability (BA) of about 75%. The ER dosage forms being investigated in this work have been described in a separate publication.[6]

The data used for the mathematical modeling in this work are based on a 4-way, 4-treatment, randomized, single-dose (100 mg), fasting, crossover study of 3 ER and 1 IR formulation variants involving 16 healthy adult volunteers. The study was designed for the purpose of IVIVC development. There was a 1-week washout period between the study periods. Plasma concentrations of the drug were determined for samples taken up to 48 hours post-drug administration for the ER formulation treatments and 24 hours for the IR formulation.

Each subject was administered 3 ER oral dosage forms corresponding to the slow (S), medium (M), and fast (F) formulations and 1 IR dosage form. All administered dosage forms belonging to a particular formulation group came from the same manufacturing batch. Dissolution profiles for each ER formulation from the aforementioned production lots were measured using USP 1 (basket) apparatus at 75 rpm in 0.1 N HCl. Average fraction dissolved *in vitro* was measured for each formulation from 12 units.

Modeling Strategy

The primary objective of this work was to demonstrate the value of stochastic deconvolution in the development of an IVIVC when applied to clinical PK data. In achieving this objective, comparisons are drawn with the most common method for IVIVC development,[7] numerical deconvolution. Both methods of deconvolution were studied using Phoenix/WinNonlin, version 6.4[8] (hereafter referred to as "Phoenix"). The solutions obtained using stochastic deconvolution were generated using the Phoenix model object with custom-code written in the Phoenix Modeling Language.

Two separate analyses were investigated: (1) a comparison of stochastic deconvolution versus numerical deconvolution when both approaches use exactly the same unit impulse response (UIR) characteristics and (2) a comparison of stochastic deconvolution versus numerical deconvolution in the development and validation of an IVIVC with various use scenarios for stochastic deconvolution.

A Comparison of Stochastic Versus Numerical Deconvolution When Both Approaches Use Exactly the Same UIR Characteristics

This analysis provides a verification of the assumption that numerical and stochastic deconvolution will yield the same result for a given data set when provided with the same inputs. To achieve this objective, the IR data (on a per subject basis) were fit to an equation described by a sum of 3 exponentials which was based on a 2-compartment PK model involving time lag and first-order absorption and elimination. This yielded the estimated macro-constants and their associated exponents ($B_1, \beta_1, B_2, \beta_2, B_3, \beta_3$, where $B_3 = -(B_1 + B_2)$) which served as direct input for numerical deconvolution. For stochastic deconvolution, the volume of distribution (V_1) normalized by the BA and the corresponding micro-constants (k_{01}, k_e, k_{21}, k_{12}, where $k_{01} = \beta_3$) were used.

The variable of interest for comparison, resulting from the application of stochastic deconvolution and numerical deconvolution, was the fraction absorbed (F_{abs}) versus time profile, the time derivative of which is the primary output variable in deconvolution and is referred to as the input rate function. It should be noted that in the present study, F_{rel} and F_{abs} are assumed to be the same, that is, the fraction dissolved *in vivo* is assumed to be equivalent to the fraction absorbed into systemic circulation, reflecting rapid absorption with dissolution as the rate-limiting step in systemic BA. This is not a requisite assumption underlying stochastic

deconvolution in general, but one that is considered suitable in this instance.

The particular numerical deconvolution approach used in Phoenix is based on "deconvolution through convolution" (DTC).[9,10] The input rate function is modeled as a piecewise linear "precursor" function convolved with an exponential "dispersion" function, the latter being essentially a normalized exponential decay.[8] The precursor function is composed of "hat-type wavelets" with support points anchored at each observation time point, as shown schematically in Figure 1. Within each "observation interval," a dose scaling factor (X_j) is defined that constitutes the fraction of the dose applied in the jth wavelet. The precursor function is defined as a linear weighted sum of the X_j and the wavelets, h_j. Figure 1 shows that at any given time, t^*, there are 2 wavelets with their respective X_j that contribute to the precursor function. Numerical deconvolution converges toward a solution for the input rate function by minimizing the sum of squared residuals based on the to-be-estimated set of parameters X_j. What is particularly important to note is that the fraction input rate is de-coupled from the dose (i.e., there is no boundedness criterion placed on $\sum X_j$), allowing for F_{abs} to exceed unity when the UIR is not derived from intravenous PK data.

Stochastic deconvolution is primarily an estimation method based on the population PK/NLME framework. Precisely which parameters are estimated is at the modeler's discretion and dependent on the complexity of the absorption–disposition model. The calculation of the input rate of drug (i.e., the deconvolution) is essentially a by-product of the estimation method. For the stochastic deconvolution being considered in this first analysis, 2-compartment disposition kinetics were assumed with first-order absorption and elimination, in line with the underlying model structure set up to fit the IR data. The following system of ODEs was solved per subject and per ER formulation:

- First-order mass transfer from the absorption compartment, with the initial condition: at $t = 0$, $A_a = 100$ mg (the administered dose of drug).

$$\frac{dA_a}{dt} = -k_a A_a \tag{1}$$

The "fractional input rate of drug" in the context of stochastic deconvolution is $-\frac{1}{D}dA_a/dt$, where D is the administered dose of drug, and therefore, the fraction absorbed, F_{abs}, is simply the time integral thereof.

- Mass transfer for the central compartment, with first-order elimination and exchange with the peripheral compartment.

$$\frac{dA_1}{dt} = k_a A_a - k_e A_1 - k_{12} A_1 + k_{21} A_2 \tag{2}$$

- Mass transfer for the peripheral compartment.

$$\frac{dA_2}{dt} = k_{12} A_1 - k_{21} A_2 \tag{3}$$

The plasma concentration is identified as the concentration in the central compartment and defined in terms of V_1:

$$C_1(t) = \frac{A_1(t)}{V_1} \tag{4}$$

In Equations 1-4, the PK parameters are fixed for each subject across all formulations by the estimates derived from fitting the IR data described earlier. Furthermore, time (t) is interpreted as "time after dose"; this begins at zero for each administration of a particular ER drug product formulation for a given subject and ends at 48 hours according to the sampling schedule. The absorption rate coefficient is modeled as a mixed effect[5]:

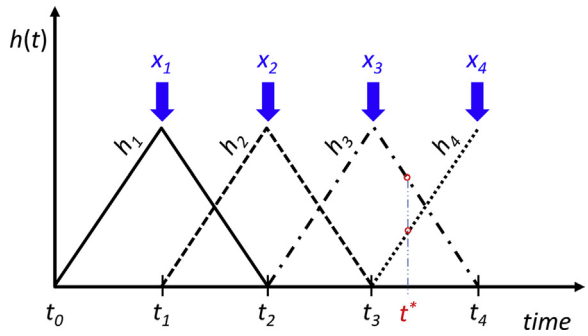

Figure 1. Schematic showing construction of "hat-type wavelets" used in Phoenix/WinNonlin's implementation of numerical deconvolution.

$$k_a(t) = \theta_{k_a} \cdot e^{\sum \eta_{k_a}(t)} \tag{5}$$

Equation 5 expresses the absorption rate coefficient as the product of its (fixed effect) population estimate, θ_{k_a}, and the exponentiated sum of random effects, $\eta_{k_a}(t)$, estimated at time points defined by the blood draw samples of the observed data. The structure defined in Equation 5 implicitly assumes that k_a is log-normally distributed. The absorption rate term $\sum \eta_{k_a}(t)$ is defined in the following manner:

$$\sum \eta_{k_a}(t) = \sum_{t_i \le t} \eta_{k_a}(t_i) \tag{6}$$

Equation 6 indicates that the value placed on the random walk for η_{k_a} at any given time is the sum of all random effects up to and including that time, that is, random effects defined at observation time points $t_i > t$ are not included in the summation. For each observation time t_i, the individual random effects for absorption are expressed as increments of a Wiener process[11]:

$$\eta_{k_a}(t_i) = w_i \cdot \sqrt{(t_i - t_{i-1})} \tag{7}$$

The term w_i is a normally distributed random variable associated with the Wiener increment, with a mean of zero and a variance (assumed to be constant) given by σ_w^2 and whose value is also estimated by the solution procedure. Between the observation times (for which there are no measured data), the random walk on k_a is held fixed. Between these increments, the ODEs presented earlier are solved.

The DTC solution estimates an input rate profile that may exceed the total dose amount, to account for the relative BA of the deconvolved profile versus the reference (UIR) profile. In contrast, the system of ODEs which form the framework of stochastic deconvolution describes a mass balance. Consequently, to ensure that stochastic deconvolution mimics numerical deconvolution, an additional random effect was included which scales the dose added to the absorption compartment at zero time. This is mathematically the same as scaling up the input rate function, as in the DTC approach.

A maximum likelihood estimate criterion was used to solve the NLME system defined earlier. An additive error model was used to build the likelihood function. The primary parameter estimates, for which a solution is sought, are the typical (population mean) values of the absorption rate coefficient for each ER formulation, 16

random effects associated with the absorption rate coefficient (one at each observed time point), a random effect on BA, the variances of all aforementioned random effects (noting that the variances of all η_{k_a} were assumed to be the same), and the residual errors associated with the error model (one per ER formulation).

A Comparison of Stochastic Versus Numerical Deconvolution in the Development and Validation of an IVIVC With Various Use Scenarios for Stochastic Deconvolution

The goal of this second analysis was to apply stochastic deconvolution as a full population PK model to the clinical PK data to develop an IVIVC. In comparison with the model structure described in the previous section, this required the following modifications/considerations:

- The PK microconstant parameters were no longer supplied to stochastic deconvolution from an external fit. Instead, stochastic deconvolution estimated these parameters "on the fly" by combining all the data (discussed subsequently).
- The random effect associated with BA, referenced in the previous section, was no longer used.
- While in the previous section only a 2-compartment PK model was considered (because of the PK micro-constant input structure), now both single and 2-compartment models were considered. The single-compartment ODEs can be obtained by setting k_{12} and k_{21} to zero in Equations 2 and 3.
- The population PK/stochastic deconvolution method was applied using all the clinical PK data (i.e., IR and ER formulations), as well as just the ER data (i.e., the IR data were withheld) to inform the estimation of parameters.

The data were combined by re-defining "time" for a given subject to include all formulation treatments. In accordance with the study plan, a 1-week washout time was prescribed to separate the respective formulation administrations, and a transformed time was defined, referred to as "relative actual time" (RAT), as expressed in Equation 8:

$$t_{\mathrm{RAT}} = (\mathrm{FID} - 1) \times 7 \times 24 + t \tag{8}$$

By staggering the dosage time in this manner, estimates were sought for a subject's V_1 and k_e that provided the best fit for all formulations. In Equation 8, t is "time after dose" and FID is the formulation identifier (1 = fast, 2 = medium, 3 = slow, 4 = IR). Residual (unabsorbed) drug was zeroed before considering the integration of the next profile (corresponding to a subject-formulation combination). The prescribed washout time in the model ensured that residual amounts of (absorbed) drug in the central compartment (and peripheral compartment, for 2-compartment descriptions) had adequate time to be cleared by the assumed first-order elimination.

Random effects were defined for volume of distribution and elimination rate coefficient (η_{V_1} and η_{k_e}, respectively) common to all formulation treatment arms and assigned to each subject. The random effects on absorption, η_{k_a}, were defined at each observation time point of the transformed time expressed in Equation 8. Thus, a unique η_{k_a} was assigned to each blood sampling time point per administered formulation. For an estimation problem involving all 4 formulations (IR and 3 ER), 68 random effects were defined to track the evolution of the absorption rate coefficient over time. The structural parameters for V_1 and k_e were defined as follows (based on an assumption of a log-normal distribution):

$$V_1 = \theta_{V_1} \cdot e^{\eta_{V_1}} \tag{9}$$

$$k_e = \theta_{k_e} \cdot e^{\eta_{k_e}} \tag{10}$$

The absorption rate coefficient was defined as in Equation 5 and the system of ODEs expressed in Equations 1-3 also applied in this instance, bearing in mind that time is now interpreted as relative actual time (t_{RAT}) as opposed to time after dose (t). For simplicity, the intercompartment rate constants, k_{21} and k_{12}, were defined as fixed effects in the case of the 2-compartment PK models. As in the previous section, an additive error model was used to build the likelihood function.

The solution to stochastic deconvolution yielded individual predictions of $F_{\mathrm{abs}}(t)$ per subject ($N = 16$) and per formulation (F, M, and S). These individual $F_{\mathrm{abs}}(t)$ solutions were then used together with the (arithmetically) averaged *in vitro* dissolution data in a naive-pooled regression based on the following IVIVC, which constitutes a linear model with constant time scaling:

$$\overline{F}_{\mathrm{abs}}(t) = A_s \, F_{\mathrm{diss}}(T_s \, t) \tag{11}$$

In Equation 11, t is the time after dose (an *in vivo* time scale), the overbar symbol in $\overline{F}_{\mathrm{abs}}$ denotes "averaged" to distinguish it from the subject-specific values. A_s and T_s are constants expressing absorption and time scaling factors (respectively), and $F_{\mathrm{diss}}(T_s \, t)$ represents the average fraction dissolved *in vitro* evaluated at a linearly transformed time $T_s \, t \, (= t_{\mathrm{vitro}})$. The naive-pooled regression estimated the parameters A_s and T_s which are shared by all formulations. Although more complex relationships could be developed with potentially better accuracy, the goal was to demonstrate a "proof of principle" for stochastic deconvolution using clinical PK data rather than develop the most accurate IVIVC. The functional relationship expressed as $F_{\mathrm{diss}}(T_s \, t)$ draws on the averaged *in vitro* dissolution data which was fitted to a Weibull function, such that

$$F_{\mathrm{diss}}(t_{\mathrm{vitro}}) = F_{\mathrm{diss},\infty}\left[1 - e^{-\left(t_{\mathrm{vitro}}/\overline{T}_{\mathrm{diss}}\right)^b}\right] \tag{12}$$

A separate nonlinear regression was used to estimate the parameters $F_{\mathrm{diss},\infty}$, $\overline{T}_{\mathrm{diss}}$, and b sorted on formulation (F, M, and S), that is, each formulation's *in vitro* release was characterized by its own specific set of parameter estimates. With the established IVIVC expressed as Equation 11, an internal validation was performed for all stochastic deconvolution scenarios which were investigated—these "scenarios" are discussed in the Results and Discussion section. The validation of the IVIVC followed the traditional approach of an arithmetically averaged relationship between fraction dissolved *in vitro* and the fraction absorbed *in vivo*. The IVIVC-predicted averaged plasma concentration–time profile, denoted $\overline{C}_1(t)$, was determined by solving the differential equation system expressed in Equations 1-4 recast in an averaged context. Thus, the rate of drug loss from the absorption compartment is now characterized by the IVIVC–Weibull function and not the absorption rate coefficient expressed in Equation 1:

$$\frac{d\overline{A}_a}{dt} = -D \, A_s \, T_s \, F_{\mathrm{diss},\infty} \frac{b}{\overline{T}_{\mathrm{diss}}} \left(\frac{T_s \, t}{\overline{T}_{\mathrm{diss}}}\right)^{b-1} e^{-\left(\frac{T_s \, t}{\overline{T}_{\mathrm{diss}}}\right)^b} \tag{13}$$

The overbar symbol in $\overline{A}_a$ denotes the averaged value based on the IVIVC, and this distinguishes this value from A_a which is subject specific and pertains to the stochastic deconvolution estimation procedure. The mass transfer for the central compartment, analogous to Equation 2, becomes:

$$\frac{d\overline{A}_1}{dt} = -\frac{d\overline{A}_a}{dt} - \widetilde{k_e}\,\overline{A}_1 - \theta_{k_{12}}\,\overline{A}_1 + \theta_{k_{21}}\overline{A}_2 \tag{14}$$

In Equation 14, $\widetilde{k_e}$ is the log-mean (or geometric mean) of the post hoc estimates of subject elimination rate coefficients. $\widetilde{k_e}$ is evaluated using the following relationship:

$$\widetilde{k_e} = \exp\left[\frac{1}{N}\sum_{i=1}^{N}\ln(k_{e,i})\right] \tag{15}$$

N denotes the number of subjects (assumed in this instance to be the same per treatment arm). The choice of the averaged metric $\widetilde{k_e}$ is premised on the fact that the individual subject k_e values are assumed to be log-normally distributed, as evidenced by the definition in Equation 10. The terms $\theta_{k_{12}}$ and $\theta_{k_{21}}$ are the (population) typical value final estimates of the intercompartmental rate constants because these parameters were defined as fixed effects. If single-compartment kinetics is assumed, $\theta_{k_{12}} = \theta_{k_{21}} = 0$. The mass transfer relationship for the peripheral compartment (for only 2-compartment kinetics) can be expressed as:

$$\frac{d\overline{A}_2}{dt} = \theta_{k_{12}}\,\overline{A}_1 - \theta_{k_{21}}\overline{A}_2 \tag{16}$$

The averaged IVIVC-predicted plasma concentration is given by:

$$\overline{C}_1(t) = \frac{\overline{A}_1(t)}{\widetilde{V_1}} \tag{17}$$

As in the case of Equation 14, $\widetilde{V_1}$ is analogously defined to the definition of the metric $\widetilde{k_e}$:

$$\widetilde{V_1} = \exp\left[\frac{1}{N}\sum_{i=1}^{N}\ln(V_{1,i})\right] \tag{18}$$

For comparative purposes, a parallel IVIVC using numerical deconvolution was also developed. Equations 11 and 12 were also used to develop the IVIVC in this instance. Because the *in vitro* data input are the same regardless of which approach is used to develop the IVIVCs, the only significant difference between stochastic deconvolution and numerical deconvolution rests with the resulting fraction absorbed profiles.

Results and Discussion

The *in vitro* and *in vivo* data sets used as the basis of the studies are shown in Figures 2 and 3, respectively, expressed as sample averages overlaid with error bars showing the standard deviation. Qualitative rank-order correlation can be confirmed by visual inspection. To gain more insight of the level of variability in the *in vivo* data, Figures 4 and 5 depict the distribution of AUC_{last} and C_{max} in the form of box plots. The individual spread of AUC_{last} and C_{max} are annotated randomly over the area of the respective boxes. Although the monotonic drop in median C_{max} is apparent in Figure 5 from the IR to the slow formulations, the median AUC_{last} of the IR, fast, and medium formulations appear constant, with a relative drop for the slow formulation. Notably for the slow formulation, one particular subject has a significantly lower AUC_{last} and C_{max}. However, this very same subject (identified with the dotted circle in Figs. 4 and 5) exhibits a behavior either very close to the median or well within the interquartile range when administered the other formulations.

A Comparison of Stochastic Deconvolution Versus Numerical Deconvolution When Both Approaches Use Exactly the Same UIR Characteristics

Figure 6 demonstrates that both approaches predict solutions for $F_{abs}(t)$ which are indistinguishable. Of particular note, the $F_{abs}(t)$ profile for subject ID "9" plateaus at just under 120% of the dose. The estimate of the cumulative input at the last observed time point is $F_{abs}(t)$ multiplied by BA ratio (in this instance) of the fast formulation's to the UIR's AUC_{last}. Therefore,

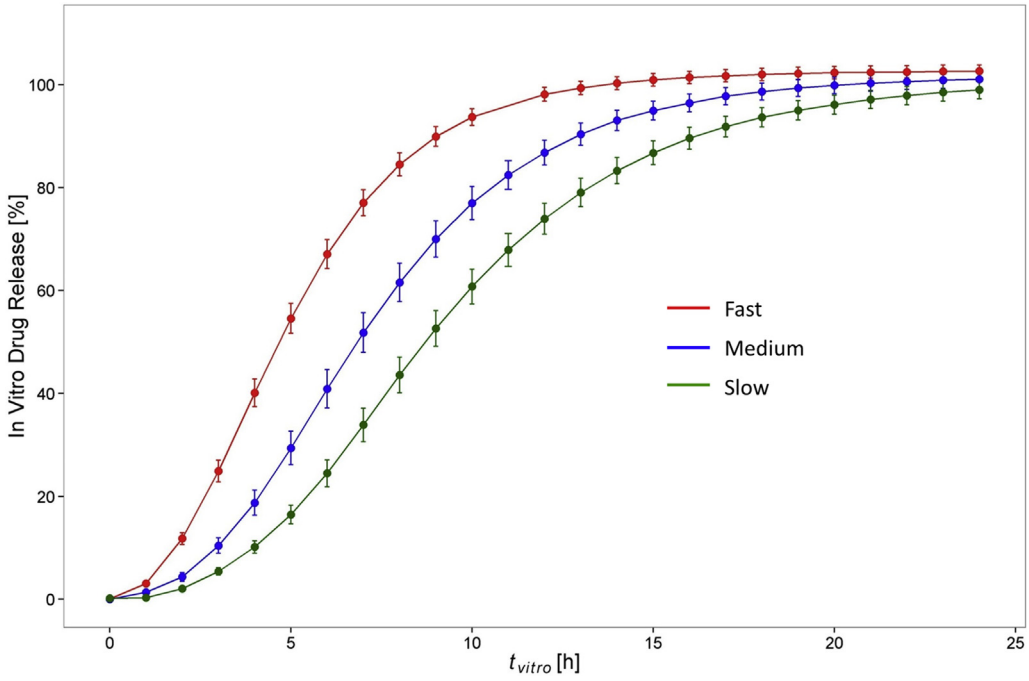

Figure 2. Observations of *in vitro* dissolution profiles for ER formulation variants with error bars showing standard deviation (based on 12 samples per formulation).

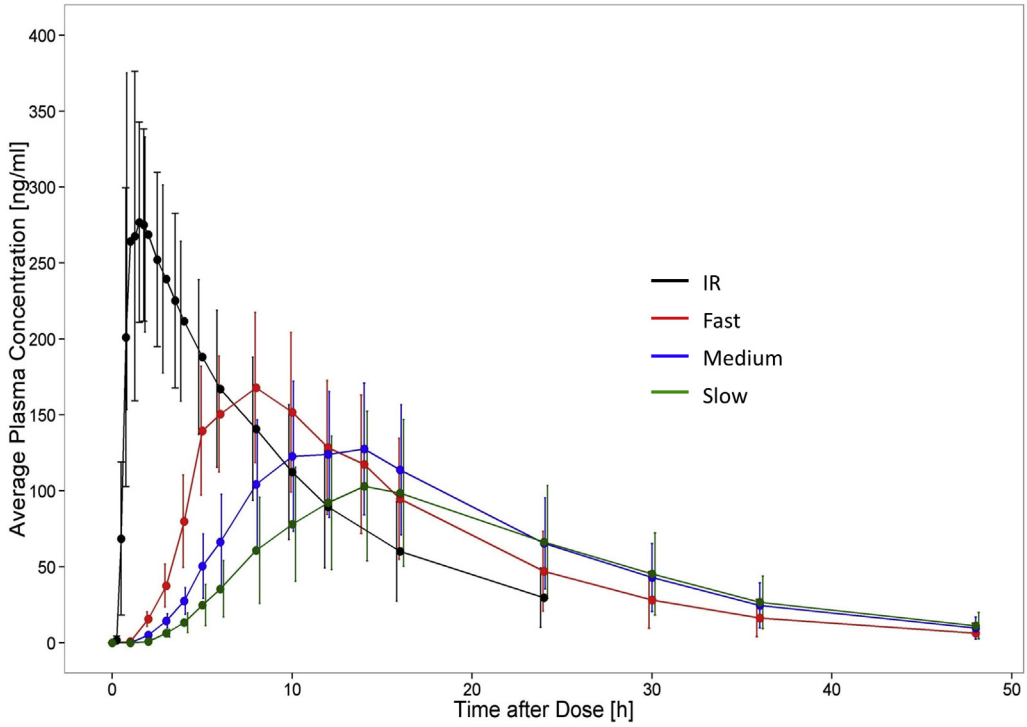

Figure 3. Observations of averaged plasma concentration–time profiles for all administered formulations (IR and ER). Error bars show standard deviation ($N = 16$).

in this particular scenario, the fast formulation has a higher exposure than its corresponding UIR. The higher exposure is a feature of the data and not a shortcoming of numerical deconvolution per se. The corresponding comparisons for the medium and slow formulations have been omitted for conciseness because they provide the same level of similarity between the 2 deconvolution approaches as seen in Figure 6 but without the visibly large $F_{abs} \approx 120\%$.

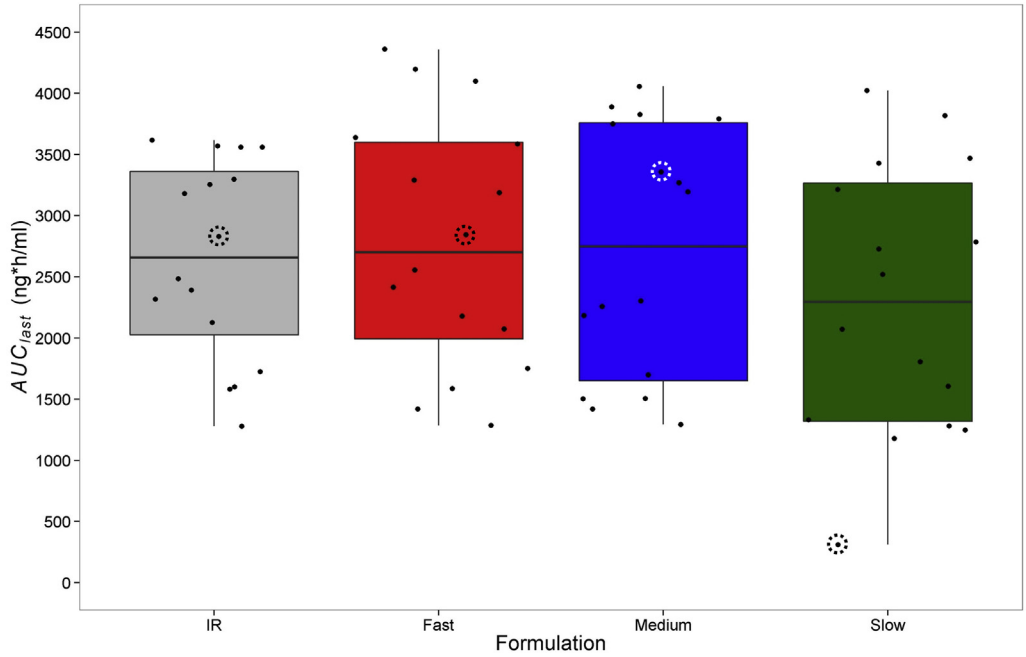

Figure 4. Box plot showing distribution of AUC_{last} from raw data amongst subjects as a function of administered drug product formulation. Each box shows the 25th and 75th percentiles (hinges) and the median. The upper and lower whiskers extend from their respective hinges to the highest and lowest values, respectively, within 1.5 times the interquartile range. The overlaid, randomly dispersed black dots represent individual AUC_{last}. The dotted circles identify the same subject across all formulations, who demonstrated a notably lower AUC_{last} when administered the slow formulation.

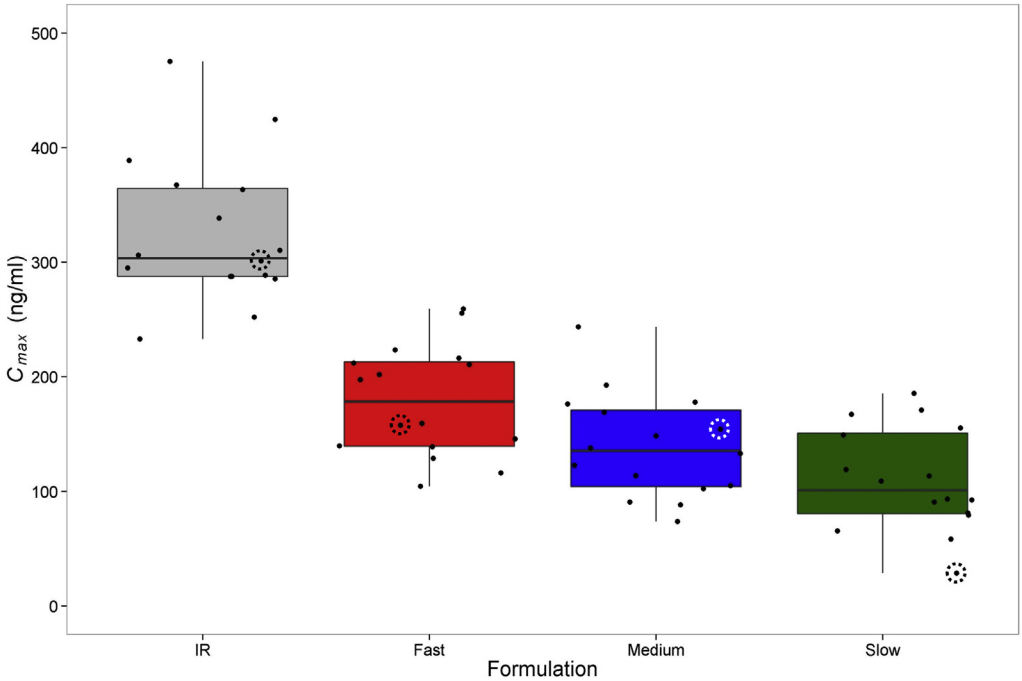

Figure 5. Box plot showing distribution of C_{max} from raw data among subjects as a function of administered drug product formulation. Each box shows the 25th and 75th percentiles (hinges) and the median. The upper and lower whiskers extend from their respective hinges to the highest and lowest values, respectively, within 1.5 times the interquartile range. The overlaid, randomly dispersed black dots represent individual C_{max}. The dotted circles identify the same subject across all formulations, who demonstrated a notably lower C_{max} when administered the slow formulation.

Comparison of the IVIVC Validation Based on Stochastic Deconvolution and Numerical Deconvolution

The IVIVC model development and validation using stochastic deconvolution in this second analysis was based on $F_{abs}(t)$ profiles stemming from 4 different modeling scenarios:

1. Using a single-compartment PK framework and *in vivo* data from the IR and all ER treatment arms to inform on the estimation of the model's structural parameters (k_a, V_1, and k_e).
2. Same as scenario 1 mentioned earlier but using *in vivo* data just from the ER treatment arm for the estimation of structural parameters.
3. Using a 2-compartment PK framework and *in vivo* data from the IR and all ER treatment arms to inform on the estimation of the model's structural parameters (k_a, V_1, k_e, k_{12}, and k_{21}).
4. Same as scenario 3 mentioned earlier but using *in vivo* data just from the ER treatment arm for the estimation of structural parameters.

All scenarios use the ER data to inform the parameter estimation but scenarios 1 and 3 also include the IR data. This was deliberately implemented to determine how well stochastic deconvolution can converge on model estimates in the event that IR data were not available.

Each of the scenarios mentioned earlier constitutes an estimation problem requiring initial estimates for the typical values ("fixed" effects) of the structural parameters, the variances of all random effects, and the residual error associated with the additive error model. The initial estimates of the typical values of the structural parameters (k_a, V_1, k_e, k_{12}, and k_{21}) were based on the respective medians derived from the 1- or 2-compartment PK model fit of the *in vivo* data.

The initial estimates of the variances of the random effects ($\omega^2_{k_e}$ and $\omega^2_{V_1}$) were chosen to allow for an initial coefficient of variation of about 30% in the structural parameters. The initial estimate for the residual error/variability (σ) was selected to be 10% of median concentration. These estimates worked well for the single-compartment scenarios (1 and 2), but the 2-compartment test cases (scenarios 3 and 4) benefitted from higher initial estimates for variance by yielding more plausible final solutions, as discussed in the paragraph given subsequently. Solution robustness was investigated by examining the effect of the choice of solver for the ODEs (stiff vs. non-stiff), optimization algorithm (FOCE-LB vs. FOCE-ELS), and variations in the initial estimates.

Several metrics were considered when determining the plausibility of any given solution. For an adequately converged solution (implying a "return code" from Phoenix's NLME solver in the range of 1 to 3), first and foremost, the magnitudes of the final typical value estimates for V_1 and k_e were assessed. This means that if these final estimates were significantly different from the plausible range of values based on the literature and the estimates of PK data fits (discussed earlier), the results would not be given further consideration. It should be noted that for the 2-compartment treatment of stochastic deconvolution, the volume of distribution at steady state (as opposed to V_1) was evaluated as the relevant comparative metric, and calculated via $V_{ss} = V_1(1 + k_{21}/k_{12})$. Literature values for V_1 and k_e are of the order of 200 L and 0.1 h^{-1}, respectively. For the other parameters (k_a, k_{12}, and k_{21}), no suitably credible comparative values could be drawn on to develop an informed assessment for their plausibility.

Given a plausible set of final parameter estimates for V_1 and k_e, the next step in the assessment procedure revolved around the consideration of the model's Akaike information criterion between successive estimation steps, the magnitude of standard errors for typical values of the structural parameters, the magnitude of the η-shrinkage associated with the random effects on V_1 and k_e and the distribution of both the random effects on V_1, k_e, and the conditional weighted residuals. Of note, not all solutions reported

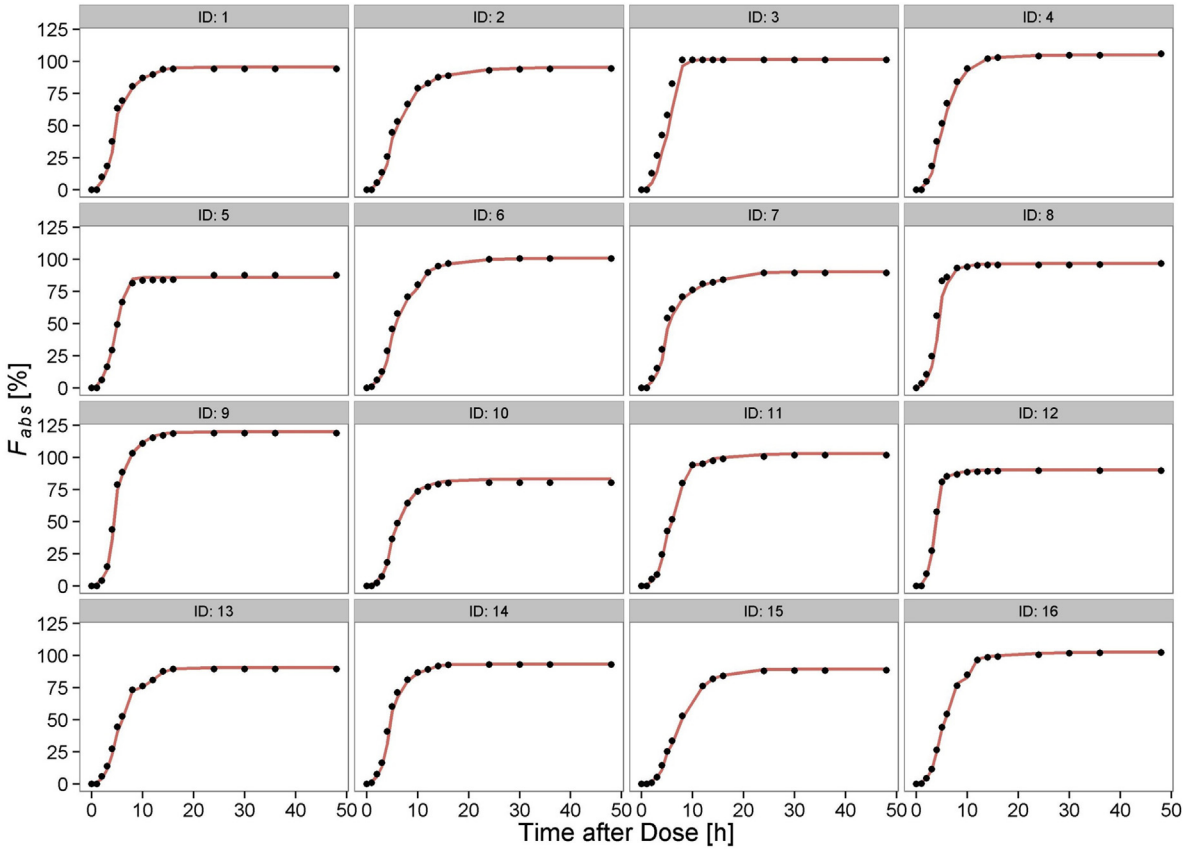

Figure 6. Comparison of calculated fraction absorbed per subject from numerical deconvolution (black dots) and stochastic deconvolution (red line) based on the same UIR input, after administration of the fast formulation.

standard errors. This could result from an overparameterized model, a solution too far from a local minimum in the likelihood function surface, or from numerical difficulties computing gradients near the solution. Due to the stability of the solutions from multiple starting points and the identifiability of many of the less optimal solutions, the latter explanation is considered to be most likely.

The modeling strategy was to begin with the initial estimates, obtain a solution, and then use these final estimates for all the calculated parameters as a starting guess for the next "iteration." This procedure was continued until a stable solution was found or at least one which best exemplified the set of assessment criteria presented earlier. Generally, it was found that using the FOCE-ELS algorithm to compute the maximum likelihood estimates coupled to the non-stiff ODE solver provided the most robust and stable results. Of the 4 modeling scenarios investigated and listed at the start of this section, the stochastic deconvolution estimation of the single-compartment PK model using IR data to inform parameter estimation (scenario 1) was found to be the most robust test case, that is, the final estimates of θ_{k_e} and θ_V were the least sensitive with respect to choice of optimization (i.e., FOCE-LB or FOCE-ELS), ODE solver algorithm, and initial estimates of the mixed-effects parameters.

Table 1 presents the final typical value estimates for the study scenarios, numbered in the same order as the list presented at the start of this section. The first 2 columns next to "Scenario" express the population mean PK parameter estimates, whereby V_1 corresponds to the single-compartment and V_{ss} to the 2-compartment models. The values in parentheses represent the percent coefficients of variation (or relative standard error) calculated from the standard errors of the respective estimates. The broad similarity of parameter estimates for volume of distribution and elimination rate coefficient for the various deconvolution scenarios implies that even when the IR data set is omitted (for scenarios 2 and 4), there is evidently enough information in the observed data to inform on the PK parameter estimates. The observation of viable PK parameter estimates in the absence of IR data is important because it suggests that stochastic deconvolution

Table 1
Estimates of PK Parameters (With Associated Standard Errors Expressed as Percentages in Parentheses) and Shrinkages for Stochastic Deconvolution Estimation Scenarios

Scenario	V_1 or V_{ss} (CV%)	k_e (CV%)	Shrinkage (−)		
	(L)	(h^{-1})	η_V	η_{k_e}	ε
1. SDcon: 1-compartment PK with IR	332 (3%)	0.12 (6.6%)	0.22	0.021	0.21
2. SDcon: 1-compartment PK without IR	324 (0.8%)	0.10 (0.9%)	0.54	0.73	0.37
3. SDcon: 2-compartment PK with IR	335 (1.1%)	0.14 (1.6%)	0.17	0.32	0.32
4. SDcon: 2-compartment PK without IR	354 (1.1%)	0.11 (1.1%)	0.41	0.08	0.41

can be used to calculate the averaged fraction absorbed without recourse to any IR data. In addition, this also implies that data for subjects in a crossover study, for whom the IR formulation was missed, can still be included as part of the analysis; for classical numerical deconvolution, the lack of an IR data set (for UIR characterization) would make the approach unworkable.

The last column in Table 1 lists the η- and ε-shrinkages. Generally, the shrinkage values (except for scenario 2) are relatively contained implying the individual data are sufficiently abundant so that individual parameter estimates mimic the true individual parameter estimates.[12] More specifically, there is confidence in the η estimates of the Ω-matrix and little concern with model "overfitting." Even in the case of scenario 2 which registers higher shrinkages across the board, the end goal of the present study was not to use the η estimates for prediction purposes in a regression/covariate model or to make inferences about parameter values but rather to inform on an averaged absorption profile that can be subsequently used to develop an IVIVC. Based on a sample size of 16 subjects, the distribution of η_{k_e} and η_{V_1} showed that a box plot straddled the zero reference line (plots not shown). Scenario 3 (2-compartment PK with IR data) exhibited the largest degree of skewness particularly with respect to η_{k_e}. Plots of conditional weighted residuals versus time after dose sorted by ER formulation showed that the distributions are centered about zero with a uniform variance (plots not shown). Regarding run times, scenario 3 (involving a total of seventy random effects) was the slowest to converge requiring just over half an hour on a Dell Precision T7500 dual processor (X5687—3.6 GHz) workstation with the message passing interface feature checked in Phoenix to take advantage of the multiple hardware cores.

The ability of stochastic deconvolution to fit the plasma concentration−time profiles of the ER formulations is demonstrated in Figures 7 and 8 for the averaged and individual cases, respectively. The plasma concentration, labeled as C_p, is understood to be equivalent to C_1 expressed in Equation 4. The figure legends provide the key to the type of deconvolution that was performed; for example "ND" denotes numerical deconvolution, "SD_1PK_IR" represents scenario 1 (single-compartment PK using IR and ER data to inform on parameter estimation) and "SD_1PK_noIR" represents scenario 2 (single-compartment PK using only ER, i.e., no IR, data to inform on parameter estimation), etc. There is minimal difference observed in the goodness of fit calculated by all the considered methods/scenarios of deconvolution. Note that the specification of the administered formulation and the y-axis scaling in Figure 8 have been deliberately omitted. The individual plasma concentration−time profiles for the remaining formulations show similar levels of fit to the one in Figure 8 and have been omitted for conciseness.

The F_{abs} profiles corresponding to Figures 7 and 8 are shown in Figures 9 and 10, respectively. On average, the difference in the F_{abs} profiles for all methods examined was small, except for the stochastic deconvolution involving a single-compartment PK without the IR data to inform the estimation process (SD_1PK_noIR) after about 10 hours. In the present model, F_{abs} is related to exposure because both methods of deconvolution attempt to fit the concentration−time data (and therefore get the "correct" AUC_{last}). Numerical deconvolution uses V_1 based off the IR formulation data, whereas stochastic deconvolution estimates V_1 across IR and ER formulations or just the latter depending on the scenario under consideration. Because the estimated V_1 values can be different, this must affect the BA, if the fitted C_p−t profiles are essentially the same; alternatively when V_1 is biased, so too may F_{abs}. The F_{abs} profiles for individual subjects in the case of the other 2 formulations (plots not shown) do not provide any other significantly different trends compared with Figure 10. It is noted, however, that $F_{abs} \gg 100\%$, was also calculated with numerical deconvolution in the present analysis as in the case of subject ID 9 in Figure 6. Stochastic deconvolution consistently calculates $F_{abs} \leq 100\%$.

The parameter estimates for A_s and T_s, as expressed in the proposed IVIVC link function (Eq. 11), resulting from the various deconvolution methods were within 3% of each other. The IVIVC-predicted (averaged) C_p−t profiles are shown in Figure 11. Table 2 lists the validation in terms of the percent prediction error (%PE). The "Predicted" column has been omitted in Table 2 to enhance its readability. It can, however, be easily recovered because the observed magnitude of the PK parameter and the %PE are known. Figure 11 and Table 2 demonstrate that there is little difference between the methods of deconvolution considered. All the deconvolution methods constituted a borderline pass/fail of the internal validation. Previous work on these same data using numerical deconvolution[6] predicted a %PE of −17% in C_{max} for the fast formulation. The difference in the value obtained in this work is attributed to the choice of the Weibull function to fit the *in vitro* data as opposed to a Hill function used in the previous work.

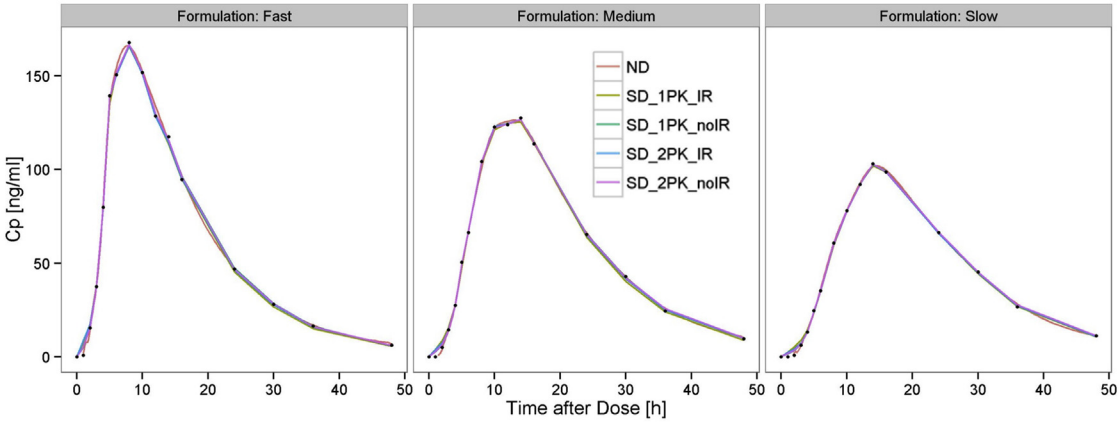

Figure 7. Comparison of averaged, predicted plasma concentration−time profiles from numerical deconvolution (ND) and various stochastic deconvolution (SD) scenarios. Dots represent the averaged observed data. SD_1PK_IR denotes stochastic deconvolution with 1-compartment PK including IR data set; SD_1PK_noIR denotes stochastic deconvolution with 1-compartment PK excluding IR data set, etc.

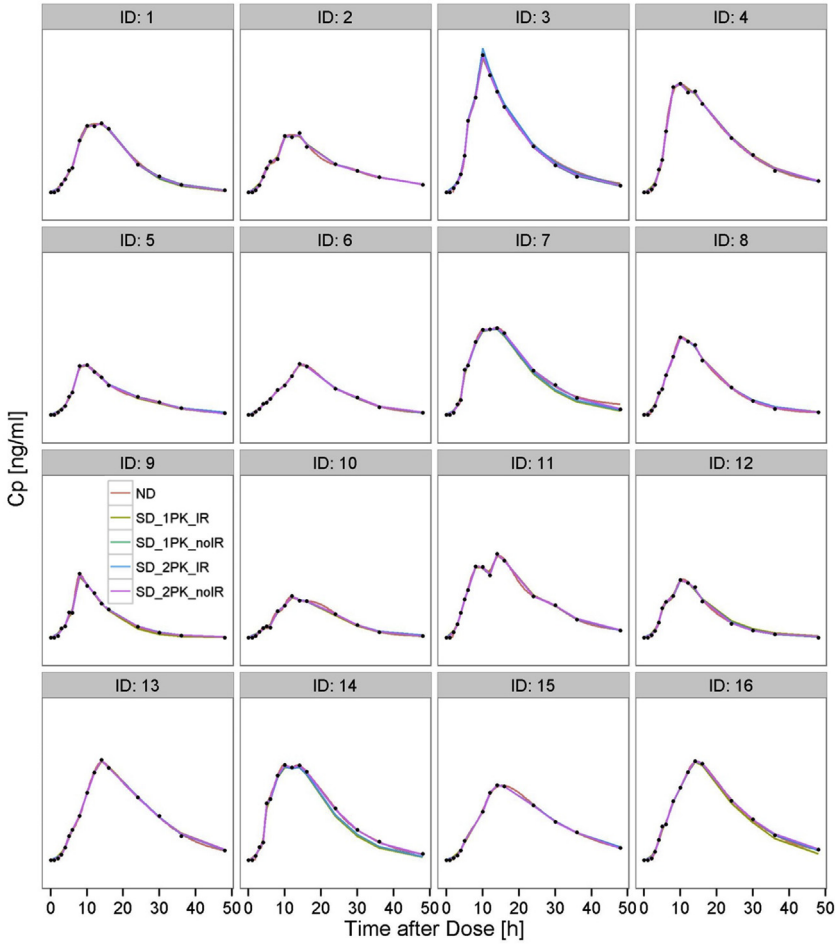

Figure 8. Comparison of individual, predicted plasma concentration–time profiles from numerical deconvolution (ND) and various stochastic deconvolution (SD) scenarios. Dots represent the individual observed data (Y-scaling omitted deliberately). SD_1PK_IR denotes stochastic deconvolution with 1-compartment PK including IR data set; SD_1PK_noIR denotes stochastic deconvolution with 1-compartment PK excluding IR data set, etc.

Conclusions

Stochastic deconvolution is a parameter estimation method that uses an NLME model to estimate an absorption rate coefficient (based on a pre-defined compartmental PK specification) defined as a random walk (Wiener process). Stochastic deconvolution serves as a diagnostic tool to inform on, rather than guess, a mapping (or link) function between the fraction-absorbed F_{abs} and the fraction of drug dissolved *in vitro* (F_{diss}) when applying 1-stage methods to IVIVC modeling, such as direct convolution and

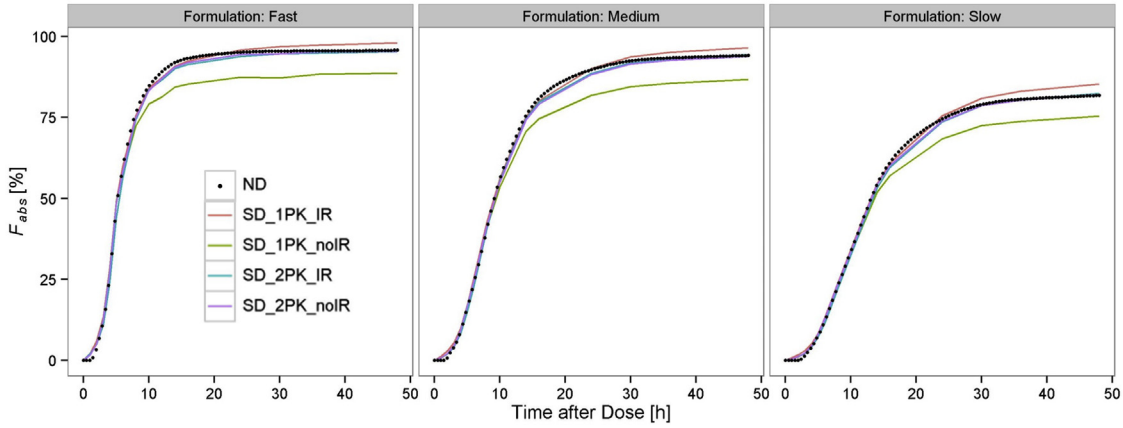

Figure 9. Average fraction absorbed profiles calculated from numerical deconvolution (ND) and various stochastic deconvolution (SD) scenarios. SD_1PK_IR denotes stochastic deconvolution with 1-compartment PK including IR data set; SD_1PK_noIR denotes stochastic deconvolution with 1-compartment PK excluding IR data set, etc.

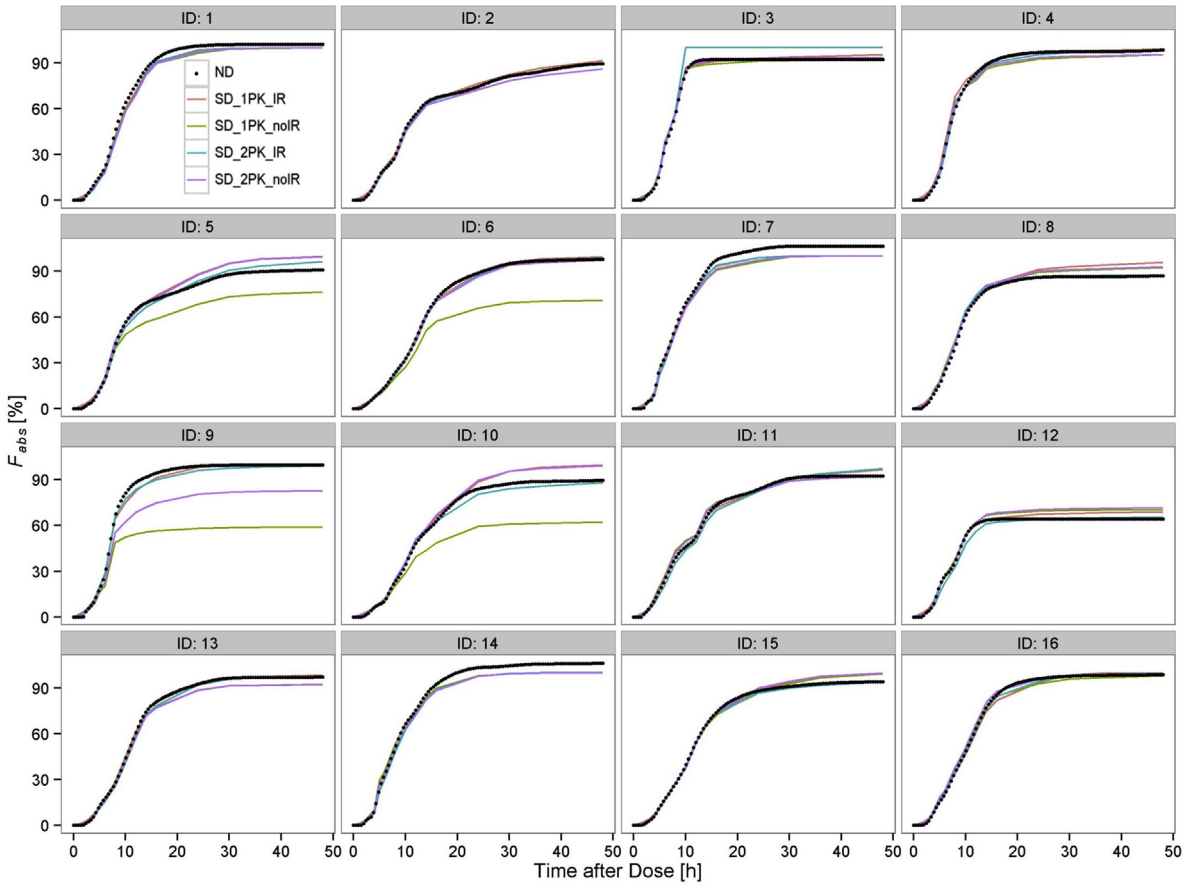

Figure 10. Individual fraction absorbed profiles for medium ER formulation calculated from numerical deconvolution (ND) and various stochastic deconvolution (SD) scenarios. SD_1PK_IR denotes stochastic deconvolution with 1-compartment PK including IR data set; SD_1PK_noIR denotes stochastic deconvolution with 1-compartment PK excluding IR data set, etc.

population IVIVC approaches. Furthermore, stochastic deconvolution is not restricted to linear, time-invariant systems. In the work presented in this study, stochastic deconvolution was applied to clinical (PK) data to assess the method's ability to predict F_{abs} profiles which can then be used to develop an IVIVC as part of a 2-stage process. A key aspect of this assessment focused on whether the clinical PK data for ER formulations could be used without additional input from IR data to estimate the parameters of the underlying model structure and inform on the F_{abs} profiles required for the IVIVC analysis. Numerical deconvolution was used as a comparative vehicle to draw on notable similarities and differences with stochastic deconvolution.

An initial analysis sought to determine under what circumstances numerical and stochastic deconvolution can be constrained

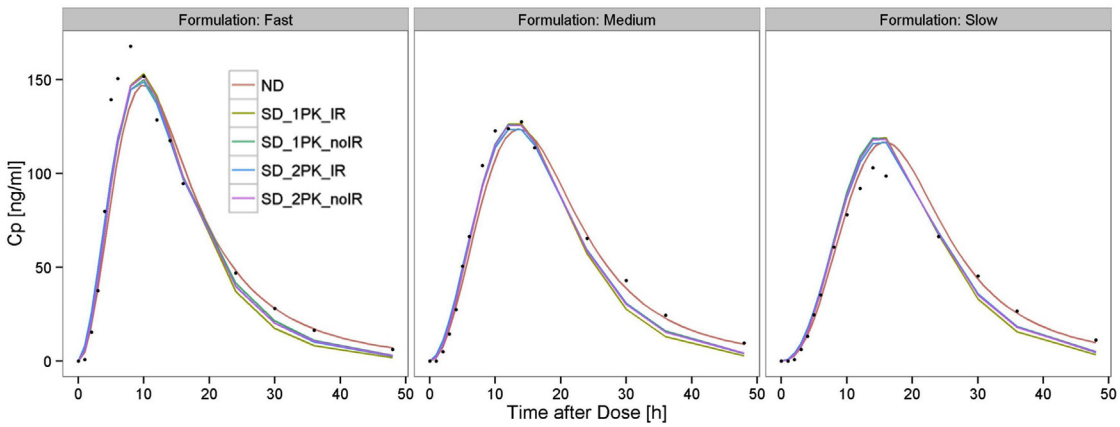

Figure 11. Comparison of averaged, predicted plasma concentration–time profiles from IVIVC based on numerical deconvolution (ND) and various stochastic deconvolution (SD) scenarios. Dots represent the averaged observed data. SD_1PK_IR denotes stochastic deconvolution with 1-compartment PK including IR data set; SD_1PK_noIR denotes stochastic deconvolution with 1-compartment PK excluding IR data set, etc.

Table 2
Table of Percent Prediction Errors (%PE) Based on Numerical Deconvolution (ND) and Various Stochastic Deconvolution (SD) Scenarios

Formulation	Parameter	Observed	Percent Prediction Error (%PE) $= \left(\frac{\text{Predicted}-\text{Observed}}{\text{Observed}}\right) \times 100$				
			SD_1PK_IR	SD_1PK_noIR	SD_2PK_IR	SD_2PK_noIR	ND
Fast	AUC_{last}	2787	−11.2	−8.8	−9.3	−9.2	−3.4
	C_{max}	168	−8.7	−10.7	−11.5	−9.5	−12.6
Medium	AUC_{last}	2716	−11.1	−8.6	−9.2	−9.2	−3.9
	C_{max}	128	−0.85	−1.0	−3.1	−1.3	−3.3
Slow	AUC_{last}	2301	−0.64	2.2	1.4	1.5	7.2
	C_{max}	103	15.5	15.4	13.0	14.9	13.1
⟨%PE⟩	AUC_{last}		7.6	6.6	6.7	6.6	4.8
	C_{max}		8.4	9.0	9.2	8.6	9.6

SD_1PK_IR, stochastic deconvolution with 1-compartment PK including IR data set; SD_1PK_noIR, denotes stochastic deconvolution with 1-compartment PK excluding IR data set, etc.
Last row expresses average (over all formulations) of the absolute %PE for the respective PK parameter.

to predict exactly the same F_{abs} profiles. Here, when both approaches were supplied with the same UIR input, the resulting F_{abs} profiles were identical. This similarity, however, could only be achieved by allowing stochastic deconvolution to adjust BA by means of a random effect multiplier. This multiplier was required because numerical deconvolution is not mathematically constrained to ensure that $F_{abs} \leq 100\%$, whereas stochastic deconvolution requires this constraint because the underlying model structure relies on a mass balance.

The subsequent analysis looked at 4 stochastic deconvolution scenarios involving a model structure for a single- and 2-compartment PK, in which IR data were either included or excluded to inform parameter estimation. In all 4 scenarios, solutions resulting in plausible estimates for V_1 and k_e could be identified which were comparable using the FOCE-ELS optimization algorithm and a non-stiff ODE solver in Phoenix (v6.4). The resulting F_{abs} profiles were then used to build an IVIVC using *in vitro* data fitted to a Weibull model. All the considered stochastic deconvolution scenarios, as well as numerical deconvolution, yielded very similar results with respect to the IVIVC validation. Given that similar results could be achieved with stochastic deconvolution without recourse to IR data was considered a positive outcome because this implies that data for subjects in a crossover study, for whom the IR formulation was missed, can still be included as part of the analysis. In contrast, for classical numerical deconvolution, the lack of an IR data set (for UIR characterization) would make the approach unworkable.

The present example looked at a drug substance whose PK was known to be linear over the dose range of interest. To challenge the utility of stochastic deconvolution further, future work will look at systems where such conditions do not prevail and where numerical deconvolution is known to fail to produce a predictive IVIVC. Another area where the current approach may be enhanced is to verify if the modeled IVIVC developed from the present 2-stage analysis can be used to inform a 1-stage population-PK IVIVC, possibly resulting in improved η- and ε-shrinkage. In this work, a "traditional validation" of the IVIVC was performed (i.e., it was based on averaged metrics for the assessment of the %PE as per the recommendations in the FDA guidance document[4]). However, the population−PK IVIVC methodology could extend the validation criteria, so that intersubject variability can be incorporated and a more rigorous picture of formulation performance evaluated.

References

1. Gillespie WR. Convolution based approaches for in-vivo in-vitro correlation modeling. *Adv Exp Med Biol*. 1997;423:53-65.
2. Van Buskirk GA, Shah V, Yacobi A, et al. Application of IVIVC in formulation development. *Dissolution Tech*. 2014;21(2):51-58.
3. US Food and Drug Administration, Center for Drug Evaluation and Research. *Guidance for Industry—SUPAC-MR: Modified Release Solid Oral Dosage Forms, CMC 8*. Silver Spring, MD: FDA; 1997. Available at: https://www.fda.gov/downloads/Drugs/Guidances/ucm070640.pdf. Accessed April 5, 2017.
4. US Food and Drug Administration, Center for Drug Evaluation and Research. Guidance For Industry—Extended Release Oral Dosage Forms: Development, Evaluation, and Application of in Vitro/In Vivo Correlations, BP 2. Silver Spring, MD: FDA; 1997. Available at: https://www.fda.gov/downloads/drugs/guidances/ucm070239.pdf. Accessed April 5, 2017.
5. Kakhi M, Chittenden J. Modeling of pharmacokinetic systems using stochastic deconvolution. *J Pharm Sci*. 2013;102:4433-4443.
6. Kakhi M, Marroum P, Chittenden J. Analysis of level A in vitro−in vivo correlations for an extended-release formulation with limited bioavailability. *Biopharm Drug Dispos*. 2013;34:262-277.
7. Suarez-Sharp S, Li M, Duan J, Shah H, Seo P. Regulatory experience with in vivo in vitro correlations (IVIVC) in new drug applications. *AAPS J*. 2016;18(6):1379-1390.
8. Pharsight Corporation. *WinNonlin/Phoenix Version 6.4* [software]. 2016.
9. Cutler DJ. Linear systems analysis in pharmacokinetics. *J Pharmacokinet Biopharm*. 1978;6(3):265-282.
10. Veng-Pedersen P, Modi NB. An algorithm for constrained deconvolution based on reparameterization. *J Pharm Sci*. 1992;81(2):175-179.
11. Jazwinski AH. *Stochastic Processes and Filtering Theory*. 1st ed. New York: Academic Press; 1970.
12. Savic RM, Karlsson MO. Importance of shrinkage in empirical Bayes estimates for diagnostics: problems and solutions. *AAPS J*. 2009;11:558-569.